Supplementary Materials
Electron Doping of Proposed Kagome Quantum Spin Liquid Produces Localized States in the Band Gap

Qihang Liu[1,2,*], Qiushi Yao[2], Z. A. Kelly[3], C. M. Pasco[3], T. M. McQueen[3,4], S. Lany[5] and Alex Zunger[1,*]

[1]*Renewable and Sustainable Energy Institute, University of Colorado, Boulder, CO 80309, USA*

[2]*Department of Physics and Shenzhen Institute for Quantum Science and Technology, Southern University of Science and Technology, Shenzhen 518055, China*

[3]*Department of Chemistry, Institute for Quantum Matter, and Department of Physics and Astronomy, The Johns Hopkins University, Baltimore, MD 21218*

[4]*Department of Materials Science and Engineering, The Johns Hopkins University, Baltimore, MD 21218*

[5]*National Renewable Energy Laboratory, Golden, Colorado 80401, USA*

[*]*E-mail:* liuqh@sustc.edu.cn; Alex.Zunger@colorado.edu

Section I. Computational Methods

The DFT calculations were performed with the projector-augmented wave (PAW) method [1] as implemented in the VASP code [2]. The generalized gradient approximation to exchange and correlation of Perdew, Burke and Ernzerhof (PBE) [3] is used for DFT level. The energy cutoff for the plane-wave basis is 400 eV, and a 6 × 6 × 4 Γ-centered Monkhorst–Pack k-mesh is used for the supercell calculations. The internal coordinates of all supercells are relaxed until the residual atomic force is smaller than 0.002 eV/Å, with hexagonal lattice parameters fixed at a = 6.55 Å, c = 9.13 Å obtained by the full relaxation of the undoped material. The electronic structure for undoped compound was also calculated from many-body perturbation theory in the GW approximation (G: Greens function, W: screened Coulomb interaction) [4], using the

projector augmented wave (PAW) implementation in the VASP code [5]. The details of the present approach are described in Refs. [6,7].

To study the *generic tendency* of $Zn_xCu_{4-x}X$ towards doping, independent of the specific dopant chemistry or whether the doped impurity is fully ionized or not, we study a model of "non-chemical doping" (analogous to gating) whereby extra "doped electrons" are added to the host crystal supercell (with a compensating positive background to assure electro-neutrality) while allowing the atoms and all electrons to self-consistently seek the new low-energy configurations. Generally, the localization of charge carriers requires an initial structural perturbation in order to break the symmetry and trigger the polaronic trapping; otherwise the lattice relaxation will end up in a local minimum with the free (delocalized) charge carrier. Our initial nudge is to elongate the 4 Cu-O bonds in one CuO_4 plane non-equivalently by ~10% and then relax the atomic positions to see if such a local symmetry breaking will stay.

Having successfully predicted a number of dopant behaviors (either polaron or extended state being the ground state) [8-10], the onsite potential approach provides us more insight on how the localization picture is related to the correction of non-linearity. For the onsite electron potential method, we add electron potentials on certain *lm* decomposed orbitals on top of the DFT+U framework, in which the Dudarev's approach [11] is used for Cu-d and Zn-d states, i.e., $(U-J)_{Cu}$ = 5 eV and $(U-J)_{Zn}$ = 6 eV, respectively. We also added a non-local external potential (NLEP) $V_{O,p} = -1$ eV on O-p orbitals for the empirical band-gap correction [12]. The onsite potential is implemented as the combination of DFT+U and NLEP method from Ref. [12]. For electron doping, the corresponding electron state potential is given by

$$V_e = \lambda_e(p_{m,\sigma}/p_{host} - 1), \quad \text{(S1)}$$

where $p_{m,\sigma}$ and p_{host} denote the target hole occupation of the m sublevel of spin σ, and the target hole occupation of the host material without doping. We determine p_{host} in Eq. (S1) to be 0.70 from the partial charge of the Cu-d orbitals of the unoccupied states. The parameter λ_e is tuned to perfectly fulfil the linearity of $E(N)$, i.e., the generalized Koopmans condition Eq. (1) of the main text.

For charged states (i.e., the non-chemical doping), the image charge corrections due to the periodic supercells are considered by using the method of Lany and Zunger [13]. For

dielectric constant that enters into the image charge corrections, our calculated electronic contribution to the static dielectric constant by DFT+U is about 3.56, based on the real part of the dielectric function □(ω) for ω → 0. The ionic contribution is calculated using density-functional perturbation theory [14]. The total dielectric constants of kagomé $ZnCu_3(OH)_6BrF$ are thus 7.75.

Section II. Calculated exchange-interaction parameters and doping effects of antiferromagnetic $ZnCu_3(OH)_6BrF$

The exchange-interaction parameters are determined by comparing total energy of different magnetic configurations obtained from DFT calculations. In a 2×2×1 supercell (24 Cu atoms), we consider four kinds of exchange interactions for simplicity, including three intralayer interactions J_1, J_2, J_d and one interlayer interaction J_i, as indicated in Fig. S1. According to Heisenberg Hamiltonian model, the total energy of a specific magnetic configuration can be written as:

$$E = E_0 + \frac{1}{4}\left(\sum_{i,j\in 1} J_1\sigma_i\sigma_j + \sum_{i,j\in 2} J_2\sigma_i\sigma_j + \sum_{i,j\in d} J_d\sigma_i\sigma_j + \sum_{i,j\in int} J_{int}\sigma_i\sigma_j\right), \quad \text{(S1)}$$

where, $\sigma_{i,j} = \pm 1$ denotes spin orientation. Table SI summarizes the exchange-interaction parameters of $ZnCu_3(OH)_6BrF$ determined from total energies of five different colinear magnetic configurations. The results show that the intralayer exchange coupling between two nearest neighboring Cu^{2+} ions is antiferromagnetic type ($J_1 > 0$) and the strongest among all, which is in consistent with the measured J in herbertsmithite [15].

We next test the non-chemical electron doping effect on one antiferromagnetic phase that has the lowest energy among the five trial configurations considered. The colinear spin orientations and the calculated density of states (DOS) upon electron doping are shown in Fig. S1a and S1c, respectively. We find fundamentally the same behavior with the magnetic structure considered in the main text, i.e., the doped electron is absorbed by a single Cu ion forming d^9-d^{10} transition and localized states inside the band gap. Therefore, the response of the material to an added electron by localizing it does not depend on the details of the spin-spin order/disorder or on entanglement. We note that all of our results presented in the main text and Supplementary Materials are based on AFM background, so the coupling between AFM and the mobile electrons are explicitly

incorporated. Studying coupling of different magnetic order is possible but outside the scope of this paper.

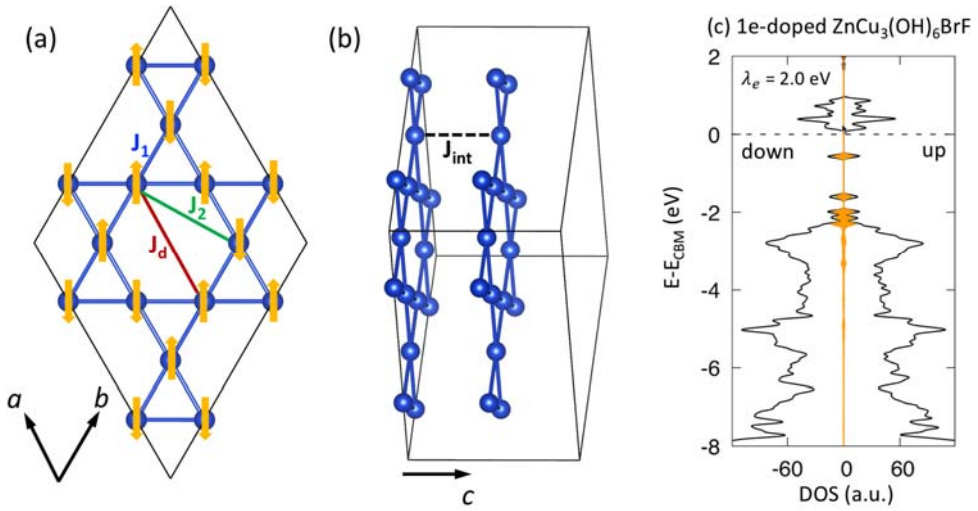

Fig. S1: (a,b) Kagome lattice of copper atoms in $ZnCu_3(OH)_6BrF$, with the exchange-interaction parameters indicated by solid (intralayer interaction) and dashed lines (interlayer interaction), respectively. (c) Calculated total density of states (DOS, black) and projected DOS of Cu^{1+} ion (orange) for doping 1 electron into a 24-atom supercell (1/3 e/Cu). The magnetic configuration has the lowest energy among the five configurations considered, with the spin orientations indicated by the orange arrows in panel (a).

Table SI: Exchange-interaction parameters of $ZnCu_3(OH)_6BrF$.

Name	$d_{Cu\text{-}Cu}$ (Å)	Exchange interaction (meV)
J_1	3.28	47.8
J_2	5.68	0.8
J_d	6.55	-0.3
J_{int}	4.57	1.7

Section III. Calculated polaron states of various electron-doped systems

To simulate a higher doping concentration, we add one electron non-chemically into a unit cell with 6 Cu atoms (corresponding to a concentration of 16.7% per Cu). The calculated DOS of electron doped $ZnCu_3(OH)_6BrF$ is shown in Fig. S2. We find that this Cu d^{10} states is still localized inside the band gap. Thus, we estimate that the electron polaron nature of kagome compound $ZnCu_3(OH)_6BrF$ is independent on different concentrations we considered.

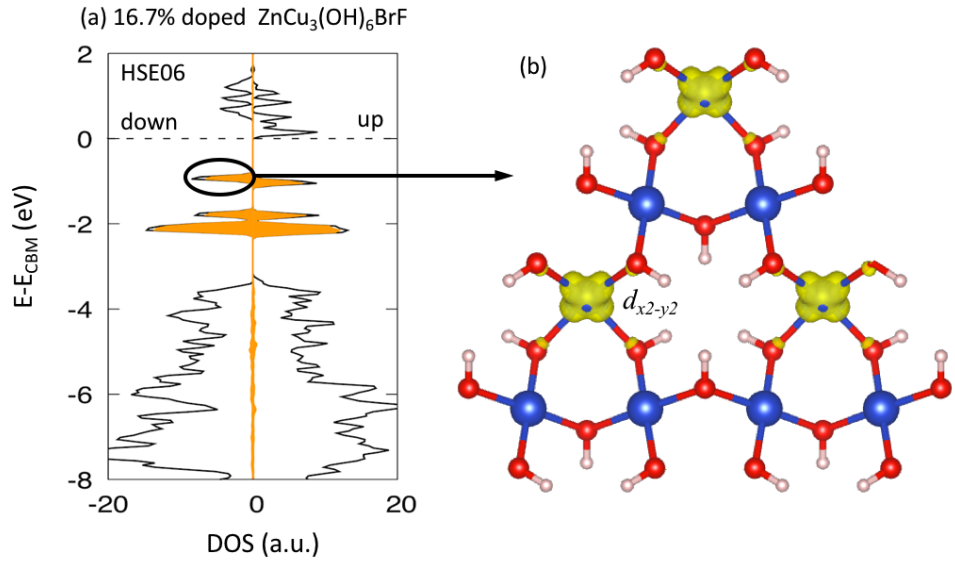

Fig. S2: (a) Calculated total density of states (DOS, black) and projected DOS of Cu^{1+} ion (orange) by hybrid functional (HSE06) for doping 1 electron non-chemically into a unit cell (1/6 electron per Cu). (b) Charge density of the highest occupied states (black circle) upon electron doping.

For $Cu_4(OH)_6BrF$ we use the recently reported orthorhombic Cmcm structure [16] with an ordered pattern of interlayer Cu^{2+} cations coupled to F atom, which resolved the previously reported disorder problem of interlayer Cu^{2+} in $P6_3/mmc$ structure [17]. The calculated DOS of electron-doped $Cu_4(OH)_6BrF$ and its derivative with 25% interlayer Zn substitution $Zn_{0.25}Cu_{3.75}(OH)_6BrF$ are shown in Supplementary Fig. S3. In both cases the doped electron is absorbed by a single Cu ion forming d^9-d^{10} transition and localized states inside the band gap. This is not surprising because the underlying kagome networks

and Cu^{2+}-OH coordination are robust with the presence of small symmetry breaking distortions.

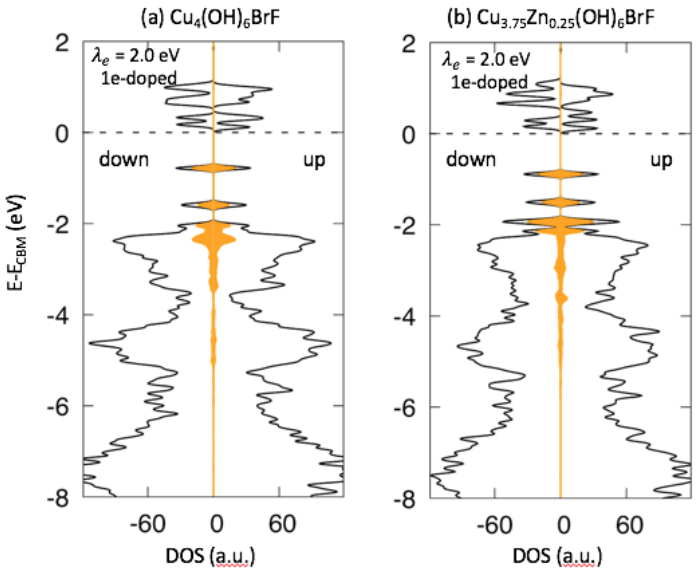

Fig. S3: Calculated total density of states (DOS, black) and projected DOS of Cu^{1+} ion (orange) for doping 1 electron non-chemically by applying onsite potential = 2 eV in (a) $Cu_4(OH)_6BrF$ and $Zn_{0.25}Cu_{3.75}(OH)_6BrF$ (b) with a Cmcm structure. Here we use a 72-atom supercell (12 kagomé Cu atoms per cell).

Section IV. Conductivity induced by polaron overlapping in electron-doped T'-phase cuprates Nd_2CuO_4

Electron doped *T'* Nd_2CuO_4 (NCO) and Pr_2CuO_4 (PCO) are typical high-temperature superconductors. Experiments show that when doped electron concentration is small (e.g., 4%), the system remains semiconducting, whereas when doping concentration reaches ~15%, the system becomes superconducting [18,19].

Pristine T' Nd_2CuO_4: Here we take *T'*-NCO as the prototype of *T'*-phase cuprates. As shown in Fig. S4a, cooper atoms in *T'*-NCO are fourfold coordinated with in-plane oxygen atoms (same as kagome compounds in the main text). Projected DOS indicates that pristine *T'* NCO refers to a positive charge-transfer band semiconductor, i.e., the conduction band is dominantly contributed by Cu-*d* state, while the valence band is the hybridization between Cu-*d* and O-*p* states (see Fig. S4b). Density functional theory at

PBE+U level [$(U-J)_{Cu}$ = 5 eV and NLEP $V_{O,p}$ = −1 eV] produces the band gap to be 0.81 eV.

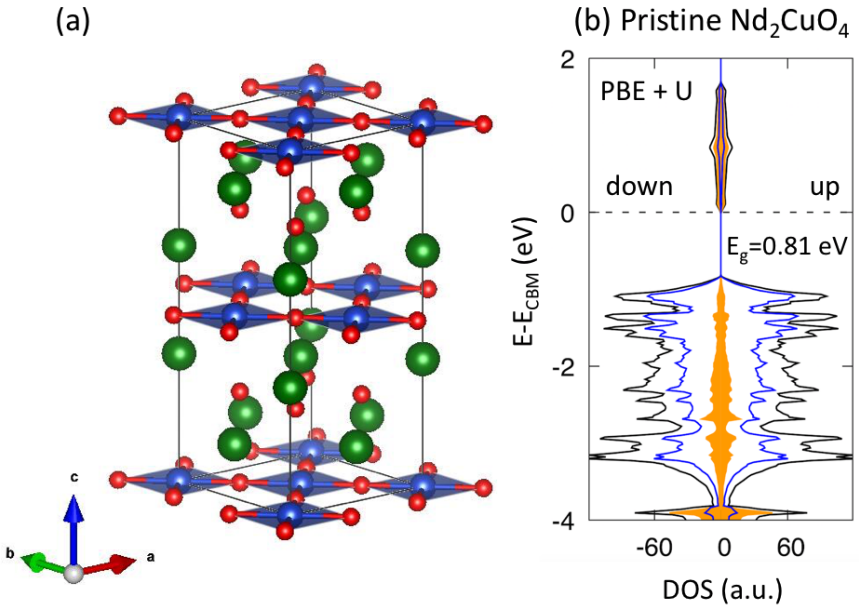

Fig. S4: (a) Crystal structure of *T'* Nd_2CuO_4. Nd, Cu and O atoms are indicated by green, blue and red balls, respectively. (b) Calculated total density of states (DOS, black) for pristine Nd_2CuO_4. The origin and blue curves denote the projected DOS of Cu and O atoms, respectively.

Electron doped T' Nd_2CuO_4: To obtain carrier concentration comparable to experiments, we construct a 2 × 2 × 1 supercell containing 32 Nd, 16 Cu and 64 O atoms. Firstly, we add one electron to the system. The resulting doping concentration is 6.25% per f.u.. According to our calculations, structure with local distortion is energetically more favorable than the symmetry structure by 13 meV/Cu. In the distorted structure, four Cu-O bonds are elongated by 0.11 Å (from 1.97 to 2.08 Å) simultaneously. Projected DOS plot (Fig. S5a) and polaron charge density (Fig. S5b) indicate that the added one electron forming a polaron with diameter about 6.8 Å (Fig. S5c), distributing on the Cu^{1+} ion and its surrounding O ligands. Additionally, the adding electron narrows the band gap to 0.57 eV. Our results show good consistent with the transport measurements, i.e., at relatively low doping concentration, *T'*-NCO remains

semiconducting [18,19]. However, taking the larger polaron size and narrowing band gap into consideration, it is reasonable to predict that *T'*-NCO may be conductive at a moderate doping concentration.

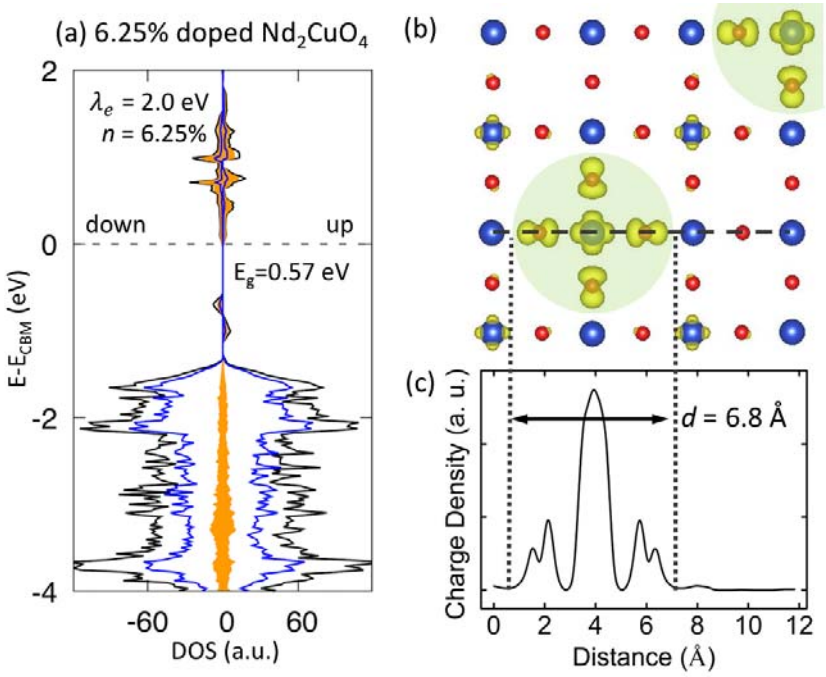

Fig. S5: (a) Calculated total DOS (black) and projected DOS of Cu (origin) and O (blue) for Nd_2CuO_4 with doping concentration of 0.0625 e^-/Cu. Onsite potential for CONL correction is 2 eV. (b) Highest occupied states charge density of the 6.25% electron-doped Nd_2CuO_4. The light green circles denote polarons distributing on Cu and coordinated O ligands. (c) Charge density along the black dash line in (b). Polaron diameter in (b) is 6.8 Å.

Secondly, we add another electron into the system, leading to a doping concentration of 12.5%. We consider three possible configurations that the two electrons are localized on two Cu atoms in the same CuO_2 plane, namely, the two Cu atoms are nearest (marked as NN, Fig. S6c and Table SII), second nearest (marked as SNN, main text Fig. 4b and Table SII) and third nearest neighbors (marked as TNN, Fig. S6d and Table SII). All the three configurations can be stabilized and the energy differences between them are very small (within 6 meV/f.u., see Table SII), indicating that all of them have a fair chance to form. NN and TNN are semiconductors with tiny band gaps of 0.05 and 0.15 eV,

respectively. On the other hand, SNN turned out to be metallic. Projected DOS (Fig. S6a and S6b) and partial charge density (Fig. S6c and S6d) indicate that the new valence band maximum is mainly distributed by two Cu and coordinated O atoms, similar to one electron doping situation (Fig. S5a and S5b). Considering the tiny band gaps and substantial polarons overlaps, NN and TNN are readily to be conductive due to polaron hopping. Thus, our calculations are consistent with experimental results that *T'* NCO undergoes semiconductor-metal/superconductor transition at relatively high doping concentration [18,19].

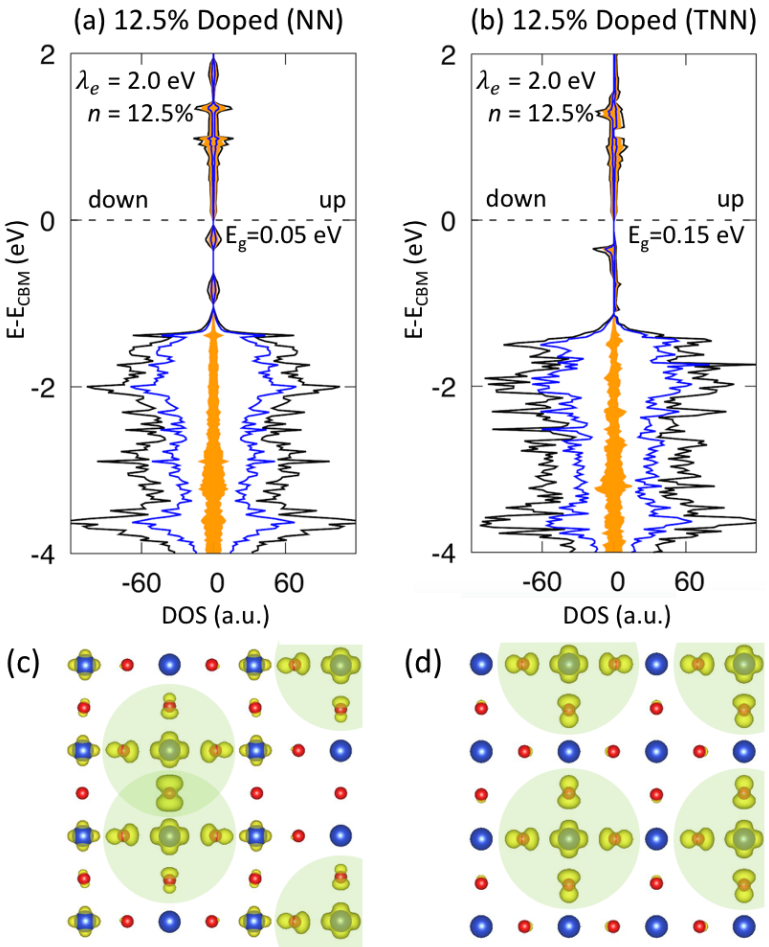

Fig. S6: Calculated total DOS (black) and projected DOS of Cu (origin) and O (blue) for 0.125 e^-/Cu doped Nd_2CuO_4 with (a) NN and (b) TNN configurations. Onsite potential for CONL correction is 2 eV. Highest occupied states charge density of the 0.125 e^-/Cu

doped Nd_2CuO_4 with (c) NN and (d) TNN configurations. The light green circles denote polarons distributing on Cu and coordinated O ligands.

Table SII: Relative energies and band gaps of 12.5% electron-doped Nd_2CuO_4 with NN, SNN and TNN configurations

Configuration	Relative Energy (meV/Cu)	Band Gap (eV)
NN	4	0.05
SNN	6	Metallic
TNN	0	0.15

References

[1] G. Kresse and D. Joubert, Phys. Rev. B **59**, 1758 (1999).

[2] G. Kresse and J. Furthmüller, Comp. Mater. Sci. **6**, 15 (1996).

[3] J. P. Perdew, K. Burke, and M. Ernzerhof, Phys. Rev. Lett. **77**, 3865 (1996).

[4] L. Hedin, Phys. Rev. **139**, A796 (1965).

[5] M. Shishkin and G. Kresse, Phys. Rev. B **74**, 035101 (2006).

[6] S. Lany, Phys. Rev. B **87**, 085112 (2013).

[7] Y. Wang, S. Lany, J. Ghanbaja, Y. Fagot-Revurat, Y. P. Chen, F. Soldera, D. Horwat, F. Mücklich, and J. F. Pierson, Phys. Rev. B **94**, 245418 (2016).

[8] P. Deák, B. Aradi, and T. Frauenheim, Phys. Rev. B **83**, 155207 (2011).

[9] H. Peng and S. Lany, Phys. Rev. B **85**, 201202 (2012).

[10] L. Stephan, J. Phys. Condens. Matter. **27**, 283203 (2015).

[11] S. L. Dudarev, G. A. Botton, S. Y. Savrasov, C. J. Humphreys, and A. P. Sutton, Phys. Rev. B **57**, 1505 (1998).

[12] S. Lany, H. Raebiger, and A. Zunger, Phys. Rev. B **77**, 241201 (2008).

[13] S. Lany and A. Zunger, Phys. Rev. B **78**, 235104 (2008).

[14] M. Gajdoš, K. Hummer, G. Kresse, J. Furthmüller, and F. Bechstedt, Phys. Rev. B **73**, 045112 (2006).

[15] J. S. Helton, K. Matan, M. P. Shores, E. A. Nytko, B. M. Bartlett, Y. Yoshida, Y. Takano, A. Suslov, Y. Qiu, J. H. Chung *et al.*, Phys. Rev. Lett. **98**, 107204 (2007).

[16] C. M. Pasco, B. A. Trump, T. T. Tran, Z. A. Kelly, C. Hoffmann, I. Heinmaa, R. Stern, and T. M. McQueen, Phys. Rev. Mater. **2**, 044406 (2018).

[17] T.-H. Han, J. Singleton, and J. A. Schlueter, Phys. Rev. Lett. **113**, 227203 (2014).

[18] Y. Tokura, H. Takagi, and S. Uchida, Nature **337**, 345 (1989).

[19] H. Takagi, S. Uchida, and Y. Tokura, Phys. Rev. Lett. **62**, 1197 (1989).